UHASSELT
KNOWLEDGE IN ACTION

Faculteit Wetenschappen

master in materiomics

Masterthesis

Novel near-infrared absorbing materials for 'truly' transparent organic photovoltaics

Maarten Iven
Scriptie ingediend tot het behalen van de graad van master in materiomics

PROMOTOR :
Prof. dr. Wouter MAES
Prof. dr. ir. Koen VANDEWAL

2023
2024

UHASSELT
KNOWLEDGE IN ACTION

www.uhasselt.be
Universiteit Hasselt
Campus Hasselt:
Martelarenlaan 42 | 3500 Hasselt
Campus Diepenbeek:
Agoralaan Gebouw D | 3590 Diepenbeek

Faculteit Wetenschappen

master in materiomics

Masterthesis

Novel near-infrared absorbing materials for 'truly' transparent organic photovoltaics

Maarten Iven

Scriptie ingediend tot het behalen van de graad van master in materiomics

PROMOTOR :

Prof. dr. Wouter MAES

Prof. dr. ir. Koen VANDEWAL

Novel near-infrared absorbing materials for truly transparent organic photovoltaics

Maarten Iven[1,*], *Kaat Valkeneers*[1,2], *Koen Vandewal*[1,2], *Wouter Maes*[1,2]

[1] Hasselt University, Institute for Materials Research (IMO-IMOMEC), Agoralaan Building D, 3590 Diepenbeek, Belgium

[2] IMEC, Associated Lab IMOMEC, Wetenschapspark 1, 3590 Diepenbeek, Belgium

E-mail: maarten.iven@student.uhasselt.be

Keywords: transparent photovoltaics, organic solar cells, non-fullerene acceptors, near-infrared absorbers, diketopyrrolopyrrole

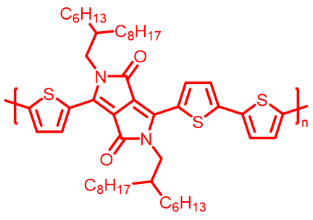

PDPP-3T

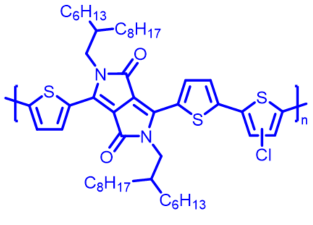

PDPP-3T(Cl)

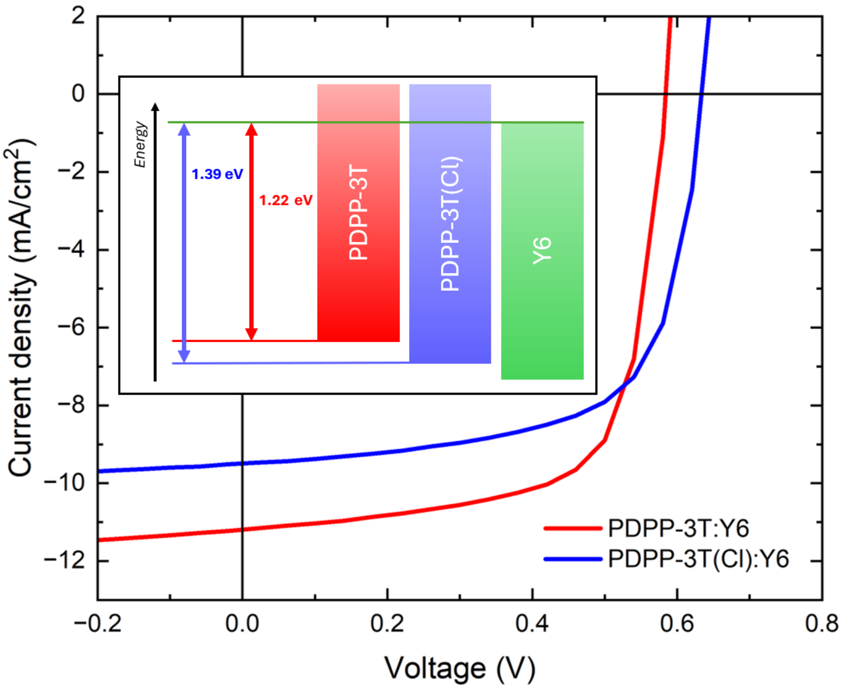

Abstract

Solar cells play a critical role in the transition from fossil fuel-based energy production to renewable energy. Opaque silicon solar cells are well established in the energy landscape nowadays. Transparent solar cells, on the other hand, could effectively function as a complementary power source, since they can, for instance, be implemented in windows of buildings and vehicles. Using organic semiconductors, these solar cells can also be thin, lightweight, and flexible, which imposes far fewer design limitations compared to conventional inorganic solar cells. Furthermore, the absorption pattern of organic semiconductors can be tuned to selectively absorb outside the visible wavelength range, which is pivotal to combine a high efficiency and transparency. Materials that fulfil these requirements are, however, rather scarcely reported. Therefore, in this work, three novel near-infrared absorbing organic materials are synthesized and their performance in photovoltaic cells is investigated. For the two novel acceptors, DOOTIC-4F and DOTIC-4F, solubility issues result in rough active layers, and therefore, unfortunately, poor solar cell performance. The novel donor polymer PDPP-3T(Cl), on the other hand, does afford a power conversion efficiency of 3.95% in combination with the near-infrared absorbing non-fullerene acceptor Y6.

Zonnecellen spelen een cruciale rol in de overgang van energieproductie op basis van fossiele brandstoffen naar hernieuwbare energiebronnen. Silicium zonnecellen zijn tegenwoordig dan ook een gevestigde waarde in het energielandschap. Transparante zonnecellen, daarentegen, zouden effectief kunnen functioneren als aanvullende energiebron, omdat ze geïntegreerd kunnen worden in o.a. ramen van gebouwen en voertuigen. Door het gebruik van organische halfgeleiders kunnen deze zonnecellen ook dun, licht en flexibel zijn, wat veel minder designbeperkingen oplevert in vergelijking met conventionele zonnecellen. Bovendien kan het absorptiepatroon van organische halfgeleiders worden afgestemd om selectief te absorberen buiten het zichtbare golflengtegebied, wat nodig is om een hoog rendement en hoge transparantie te combineren. Materialen die aan deze eisen voldoen zijn echter vrij weinig beschreven. Daarom zijn in dit werk drie nieuwe nabij-infrarood absorberende materialen gesynthetiseerd en werden hun prestaties in fotovoltaïsche cellen onderzocht. Voor de twee nieuwe acceptoren, DOOTIC-4F en DOTIC-4F, resulteren oplosbaarheidsproblemen in ruwe actieve lagen en daardoor helaas in slechte efficiënties. Het nieuwe donorpolymeer PDPP-3T(Cl), daarentegen, haalt een efficiëntie van 3,95% in combinatie met de nabij-infrarood absorberende niet-fullereen acceptor Y6.

1. Introduction

The energy transition away from fossil fuels is currently one of the most important goals of our society. Solar energy, which is one of the main renewable energy sources, has already experienced remarkable growth over the last decades. It is considered one of the major successes of the past decade, and could accelerate energy transitions around the world. [1] Conventional silicon solar panels are well represented in the energy landscape nowadays but are typically heavy and bulky and therefore not suitable in every location. Organic solar panels, on the contrary, can be thin, lightweight, and flexible. This causes them to have far fewer design restrictions compared to conventional solar cells. [2] Transparent solar panels, by extension, have even more potential applications, as even windows could be covered or replaced with solar panels, without it being intrusive. [3] The extra applications transparent solar cells provide, have the potential to considerably increase solar energy production, not only in urban areas, but also by covering crops or farmland. [4]

Transparent solar cells can be designed *via* wavelength-selective or non-wavelength-selective approaches (**Figure 1**). The non-wavelength-selective strategies apply specific device designs to achieve certain levels of transparency. These designs include using very thin layers of the photovoltaic (PV) material or dividing the surface area into small photovoltaic and non-photovoltaic regions. [5] The transparency of these devices is limited however, as they still partially absorb visible light. [6] The wavelength selective approach, on the other hand, is specific to organic solar cells (OSCs). The bandgap of the organic photoactive materials can be tuned to absorb selectively outside of the visible region to realise ‘truly’ transparent solar cells. Since 51% of the energy output from sunlight is located in the near-infrared (NIR) wavelength range (> 700 nm), and just 2% in the ultraviolet (UV) (< 400 nm), the focus for these solar cells is mostly on utilizing NIR light for photon harvesting. [7] As a result, this method requires organic semiconductors that show high absorption in the NIR, but minimal absorption in the visible light range.

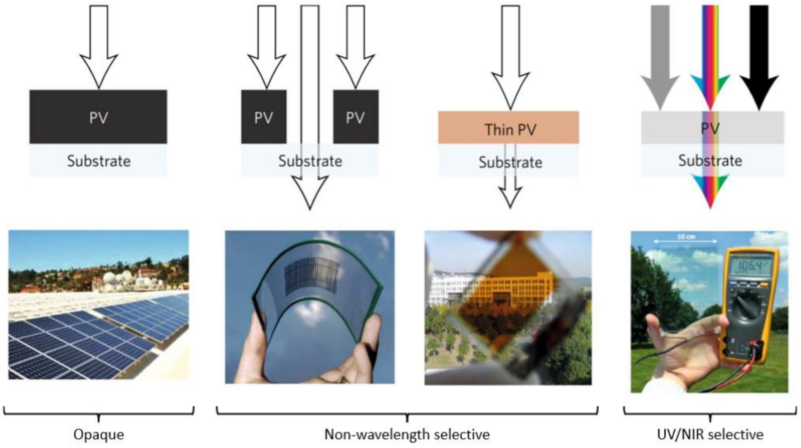

Figure 1. Design strategies for transparent solar cells. [6]

The two key parameters to evaluate transparent solar cells are the power conversion efficiency (PCE) and the visible light transmittance (VLT). The PCE is the same parameter that is used for conventional solar cells, and represents the amount of power the solar cell can generate (calculated as the product of the short circuit current density (J_{sc}), the open-circuit voltage (V_{oc}), and the fill factor (FF)) compared to the power of the incident solar spectrum (P_0) (**Equation 1**). [8]

$$PCE = \frac{J_{SC} \cdot V_{OC} \cdot \mathrm{FF}}{\mathrm{P}_0} \tag{1}$$

The VLT is a measure of transparency to the human eye, and is calculated as the integration of the transmission spectrum ($T(\lambda)$) and the AM 1.5G photon flux weighted against the photopic response of the human eye ($V(\lambda)$). The full formula is given in **Equation 2**. [8]

$$VLT = \frac{\int T(\lambda) \cdot V(\lambda) \cdot \mathrm{AM1.5G}(\lambda) \mathrm{d}\lambda}{\int V(\lambda) \cdot \mathrm{AM1.5G}(\lambda) \mathrm{d}\lambda} \tag{2}$$

A third metric, the light utilization efficiency (LUE), is the product of the PCE and VLT and provides a measure to compare transparent solar cells with a different VLT. [8]

There is, however, little published research on transparent OSCs combining a donor and an acceptor material that both absorb in the NIR range. Xie *et al.* tested the combination of the low bandgap donor polymer PDTP-DFBT, with an optical bandgap (E_g^{opt}) of 1.4 eV, and the non-fullerene acceptor (NFA) FOIC, with an E_g^{opt} of 1.32 eV, to fabricate highly transparent OSCs.

They obtained a VLT of 52% and a PCE of 4.2% with a thin silver transparent electrode. Additionally, by using an extra MoO$_3$ antireflective layer on top, the VLT could be improved to 61.5% while maintaining a decent PCE of 3.5%. [3] Lee *et al.* studied a NIR harvesting bulk heterojunction blend consisting of PDPP-2T as a donor polymer and the narrow bandgap IEICO-4F as acceptor, and achieved a PCE of 5.74% with a VLT of 60%. [9] The latest example was described by Yoon *et al.* in 2023. [10] They designed two new NIR absorbing donor polymers based on cyclopentadithiophene. Semi-transparent OSCs prepared from this donor polymer achieved a PCE of 9.9% and a VLT of 40.4% in combination with Y6, leading to an outstanding LUE of 4.0%. [10] Even though these initial results are promising, it remains very difficult to find an optimum combination of two narrow bandgap materials for OSCs.

Therefore, in this work, a novel NIR-absorbing conjugated donor polymer was synthesized, as well as two novel NFAs. The two novel NFAs are derivatives of COTIC-4F (**Figure 2**), an NFA that has previously been described by Lee *et al.*, and shows a narrow optical gap of 1.10 eV. [11] To further push the absorption of this NFA toward longer wavelengths, the 4*H*-cyclopenta[2,1-*b*:3,4-*b'*]dithiophene (CPDT) core of COTIC-4F was replaced by stronger electron donating groups, 5*H*-dithieno[3,2-*b*:2',3'-*d*]pyran (DTP(O)) and 4*H*-dithieno[3,2-*b*:2',3'-*d*]pyrrole (DTP), to form DOOTIC-4F and DOTIC-4F, respectively. [12] Unfortunately, solubility issues of these NFAs in common organic solvents complicated device processing and led to a rough absorber layer, and therefore, poor OSC performances. The envisaged donor polymer is a derivative of PDPP-3T [13] (**Figure 2**), based on the strong electron withdrawing diketopyrrolopyrrole (DPP) building block. [14] In combination with Y16F as acceptor, this polymer achieved a PCE of 7.78% with a V_{OC} of 0.64 V. [15] In order to improve this performance, the thiophene monomer was replaced with a chlorinated thiophene to obtain PDPP-3T(Cl). This lead to a lower highest occupied molecular orbital (HOMO) energy level of the resulting polymer, and therefore to a higher V_{OC} of the final device. The optimized solar cells using a PDPP-3T(Cl):Y6 blend, achieved a PCE of 3.95%.

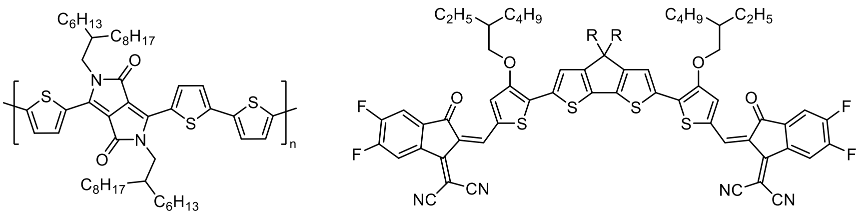

PDPP-3T

COTIC-4F (R = 2-ethylhexyl)

Figure 2. Conjugated donor polymer PDPP-3T and narrow bandgap NFA COTIC-4F.

2. Results and discussion

2.1. Synthesis and characterization

The synthesis of DOOTIC-4F and DOTIC-4F was based on a procedure reported by the group of Bazan, who described the synthesis of COTIC-4F (**Scheme 1**). [11, 16] It started with a freshly prepared donor core, which is DTP(O) [17] (**1**) in the case of DOOTIC-4F and DTP [18] (**6**) in the case of DOTIC-4F. The donor was first functionalized with trimethyltin groups using *n*-butyllithium (*n*-BuLi) and trimethyltin chloride in THF, to obtain compounds **2** and **7**. Subsequently, compounds **4** and **8** were formed from a Stille coupling of the functionalized donor core with two functional thiophene linkers **3**, using $Pd(PPh_3)_4$ as a catalyst. These precursors were then decorated with two malononitrile based end groups **5** in a Knoevenagel condensation, using pyridine as a base, to form DOOTIC-4F and DOTIC-4F, respectively. [16] The structures were confirmed by proton nuclear magnetic resonance spectrometry (^{1}H-NMR) and matrix-assisted laser desorption/ionization - time of flight (MALDI-ToF) mass spectrometry (**Figure S1-S4**). Unfortunately, the poor solubility of these NFAs in organic solvents seriously complicated the purification of the final products and led to a relatively poor overall yield of the DOTIC NFA.

PDPP-3T(Cl) was prepared according to literature *via* a Stille polymerization of a dibrominated DPP monomer **9** and 2,5-trimethylstannyl-3-chlorothiophene (**10**). [19] The synthesis of DPP monomer **9** is depicted in **Scheme S4** [20], and started with a condensation reaction of diethyl succinate with two equivalents of thiophene-2-carbonitrile to form the DPP core. 2-Hexyldecyl side chains were subsequently added, by reacting this compound and the respective bromoalkane with K_2CO_3 in dioxane. Bromine functionalization was then accomplished using *N*-bromosuccinimide (NBS) in $CHCl_3$. **Scheme S5** illustrates the synthesis of the novel (3-chlorothiophene-2,5-diyl)bis(trimethylstannane) monomer (**10**). Commercial 3-chlorothiophene was deprotonated using lithium diisopropylamide (LDA) and functionalized with trimethyltin chloride. The polymerization was conducted three times (**Table S1**). The molar masses of these polymers were measured *via* high-temperature gel permeation chromatography, and the outcome was susceptible to the concentration and reaction time of the polymerization (**Table S1, Figure S7**). Using a concentration of 0.26 M and a reaction time of 64 h, the final polymer could be obtained with a number-average molar mass of 26.7 kDa.

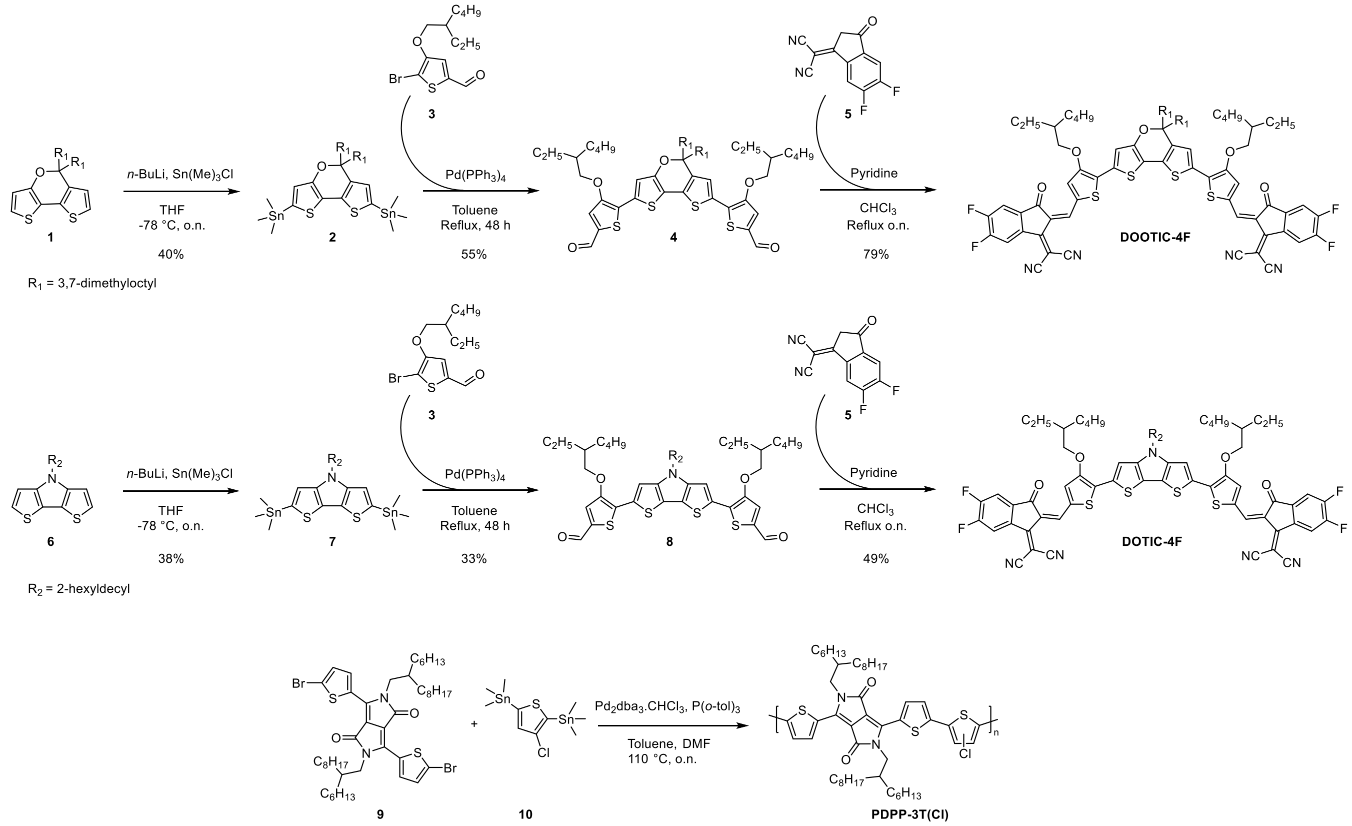

Scheme 1. Synthesis of the NFAs DOOTIC-4F and DOTIC-4F, and the donor polymer PDPP-3T(Cl) (o.n. = overnight).

Figure 3 (A) shows the absorption profiles of COTIC-4F, DOOTIC-4F, and DOTIC-4F in chloroform solution and in film. Both novel NFAs show minimal absorption in the 400-650 nm range and strong absorption peaks beyond 700 nm. The poor absorption in the visible wavelength range renders them promising materials for transparent OSCs. In solution, COTIC-4F has an absorption maximum at 876 nm, where DOOTIC-4F and DOTIC-4F show slightly redshifted maxima of 890 and 883 nm, respectively. The observed redshift scales with increasing electron donating character of the core, with DTP(O) causing a slightly larger shift than DTP. [12] In thin films, the redshift of the absorption is less pronounced, with peak values at 991 and 994 nm for COTIC-4F and DOOTIC-4F, respectively. However, DOTIC-4F shows a much broader absorption peak than COTIC-4F and DOOTIC-4F, with a maximum at 963 nm. Due to the poor solubility of the new NFAs in chlorobenzene, no thin-film absorption coefficients could be calculated, as no homogeneous films could be deposited.

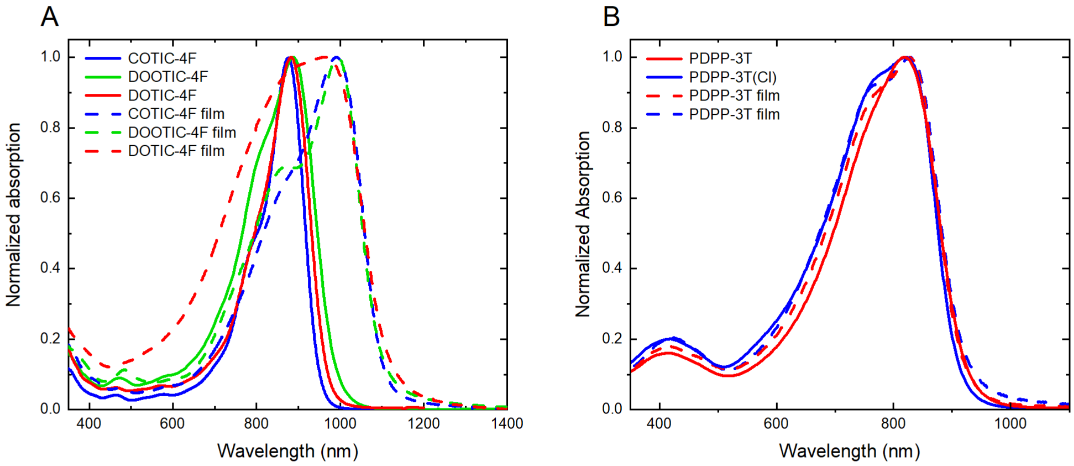

Figure 3. Normalized UV-Vis-NIR absorption spectra for (A) COTIC-4F (blue), DOOTIC-4F (green) and DOTIC-4F (red) in chloroform solution (solid lines) and in film (dashed lines) and (B) for PDPP-3T (red) and PDPP-3T (Cl) (blue) in chloroform solution (solid lines) and in film (dashed lines).

The absorption profiles of PDPP-3T and PDPP-3T(Cl) are depicted in **Figure 3** (B) and show no significant difference between the original PDPP-3T polymer and the novel PDPP-3T(Cl) polymer in chloroform solution nor in film. Both polymers show lower absorption in the 400-600 nm range and a strong absorption peak around 820 nm. The absorption coefficients were also determined for both PDPP-3T and PDPP-3T(Cl). The results depicted in **Figure S8** show that PDPP-3T(Cl) absorbs slightly weaker than PDPP-3T.

The frontier molecular orbital energy levels of the new materials were determined *via* cyclic voltammetry and the results are listed in **Table 1**. Although the envisaged redshift of the novel NFAs compared to COTIC-4F was present in the absorption spectrum, the electrochemical bandgap (ΔE_{EC}) of the NFAs did not decrease. On the contrary, both DOOTIC-4F and DOTIC-4F show a higher ΔE_{EC} than COTIC-4F. The optical bandgap ($\Delta E_{\mathrm{optical}}$) is similar for the three NFAs, as the absorption redshift in film is only a few nanometers. Aside from the bandgap, a lower HOMO energy level was obtained for DOOTIC-4F (-5.54 eV compared to -5.45 eV for COTIC-4F), while the HOMO level was not significantly altered for DOTIC-4F.

Table 1. Overview of the optical and electrochemical properties of COTIC-4F, DOOTIC-4F, DOTIC-4F, PDPP-3T and PDPP-3T(Cl).

Material	HOMO (eV)	LUMO (eV)	ΔE_{EC} (eV)	$\Delta E_{optical}$ (eV)	$\lambda_{max,sol.}$ (nm)	$\lambda_{max,film}$ (nm)	M_n (kDa)	$Đ$
COTIC-4F	-5.45	-4.22	1.23	1.13	876	991	-	-
DOOTIC-4F	-5.54	-4.18	1.36	1.13	890	994	-	-
DOTIC-4F	-5.43	-4.20	1.24	1.13	883	993	-	-
PDPP-3T	-5.32	-3.58	1.75	1.31	818	827	46.8	2.7
PDPP-3T(Cl)	-5.49	-3.56	1.92	1.34	821	829	26.7	1.9

The novel PDPP-3T(Cl) donor polymer shows a lower HOMO energy level than PDPP-3T, as expected, while the lowest unoccupied molecular orbital (LUMO) energy level remains relatively unchanged. The ΔE_{EC} increases for PDPP-3T(Cl), even though the absorption spectra of PDPP-3T and PDPP-3T(Cl) are very similar.

2.2. Photovoltaic performance

The photovoltaic performance of the novel materials was evaluated by fabricating OSCs using an inverted structure (glass/ITO/ZnO/active layer/MoO_3/Ag). The photovoltaic parameters are listed in **Table 2** (for the NFAs), and **Table 3** and **4** (for PDPP-3T(Cl) and PDPP-3T). In a first attempt, a donor-acceptor combination of the novel materials (DOOTIC-4F and PDPP-3T(Cl)) was tested in OSCs but no decent *J-V* curve could be extracted from these devices. Therefore, other donor-acceptor combinations were investigated.

The NFAs were tested with PTB7-Th as the donor material, as reported by Lee *et al.* [16] The reference devices with COTIC-4F have a comparable V_{OC} and fill factor to those published in literature. The J_{SC}, on the other hand, was lower (16.1 mA/cm^2 compared to 20.6 mA/cm^2 in literature). As a result, the PCE of the reference devices was only 5.72 % (compared to 7.3 % for the literature devices). The devices based on the DOOTIC-4F:PTB7-Th blend showed a slightly lower V_{OC} (0.52 V compared to 0.56 V), despite the higher LUMO level of DOOTIC-4F (-4.18 eV compared to -4.22 eV for COTIC-4F). Furthermore, the J_{sc} dropped drastically (0.68 mA/cm^2 compared to 16.1 mA/cm^2), which resulted in a PCE of only 0.12%. To rule out a possible energy level mismatch, the combination with the donor polymer PDPP-3T (which has a higher HOMO level than PTB7-Th), was also investigated. Unfortunately, the devices using the DOOTIC-4F:PDPP-3T blend also performed significantly worse than those based on COTIC-4F:PDPP-3T. The V_{OC} was lower (0.42 V compared to 0.55 V), and, the devices again yielded almost no current. As a result, the PCE of the devices using DOOTIC-4F is only 0.35 % compared to 2.09% for the devices based on COTIC-4F. Even though the active layers looked smooth, the poor solubility of DOOTIC-4F, compared to COTIC-4F, may hinder the formation of a proper morphology of the active layer.

Table 2. Photovoltaic parameters for the solar cells based on COTIC-4F and DOOTIC-4F.

Blend	J_{SC} **(mA/cm^2)**	V_{OC} **(V)**	**FF (%)**	**PCE (%)**
COTIC-4F:PTB7-Th	16.1	0.56	63	5.72
DOOTIC-4F:PTB7-Th	0.68	0.52	34	0.12
COTIC-4F:PDPP-3T	5.88	0.55	65	2.09
DOOTIC-4F:PDPP-3T	0.21	0.42	41	0.35

To evaluate the surface morphology of the active layer, atomic force microscopy (AFM) measurements were performed (**Figure 6**). The average roughness and root mean square roughness were significantly higher for the active layer based on DOOTIC-4F (14.33 nm and 18.15 nm compared to 0.68 nm and 0.85 nm, for COTIC-4F). This may point to a suboptimal morphology for the DOOTIC-4F:PTB7-Th absorber layer, which is probably caused by the poor solubility of the NFA in chlorobenzene. Since the poor performance of the devices based on DOOTIC-4F is most likely caused by its poor solubility in organic solvents, devices using DOTIC-4F, of which the solubility is also a problem, were not investigated.

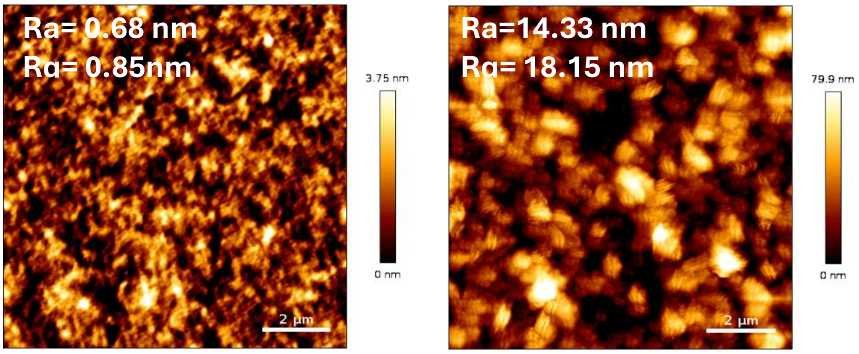

Figure 6. AFM images of the COTIC-4F:PTB7-Th (left) and DOOTIC-4F:PTB7-Th (right) photoactive layers.

The novel donor polymer was tested in OSCs, in combination with four different commercial NIR absorbing acceptors, FOIC, Y6, Y16F, and IEICO. Of these blends, PDPP-3T(Cl):Y6 performed significantly better than the other combinations, with a PCE of 3.25%. Therefore, this combination was further optimized (**Table 3**). For comparison, devices based on an active layer with the non-fluorinated analogue (PDPP-3T:Y6) were optimized as well (**Table 4**). To optimize the OSCs, the donor-acceptor (D:A) ratio, additive concentration of chlorobenzene (CB), and annealing temperature were varied. Changing the D:A ratio mainly had an impact on the FF and J_{SC} of the devices, and the optimum conditions were a 1:1 ratio for PDPP-3T(Cl):Y6 and a 1:2 ratio for PDPP-3T:Y6. The addition of CB (in 1, 3, and 5 wt%) generally resulted in a lowering of the V_{OC}. In the case of the PDPP-3T(Cl)-based devices, this also enhanced the J_{SC}, which resulted in an improved PCE of 3.85% with 1 wt% CB. For the PDPP-3T-based devices, on the other hand, adding CB generally lowered the final PCE of the devices and further optimization was done without the addition of CB. Additionally, thermal annealing further improved the FF and J_{SC}, and therefore overall efficiency of the devices. The optimal conditions for the reference PDPP-3T-based devices are a D:A ratio of 1:2 and annealing at 130 °C for 7 min. A PCE of 4.45% was measured for these devices, with a J_{sc} of 11.19 mA/cm^2, a V_{OC} of 0.58 V and a FF of 68%. For the PDPP-3T(Cl) blend, the optimal processing conditions are a D:A ratio of 1:1, with a 1% additive concentration of CB and an annealing for 7 min at 160 °C. Using these conditions, the PDPP-3T(Cl) based solar cells achieved an improved J_{sc} of 9.49 mA/cm^2 and a V_{oc} of 0.63 V, with a FF of 66% and a respectable PCE of 3.95%. To conclude, even though the V_{OC} could be enhanced by chlorinating the polymer backbone, the devices based on the original polymer (PDPP-3T) still performed better due to a higher J_{SC}.

Table 3. Optimization of the photovoltaic properties for solar cells based on PDPP-3T(Cl).

Acceptor	**D:A ratio (wt:wt)**	**CB (%)**	**Ann. T (°C)**	**J_{SC} (mA/cm^2)**	**V_{OC} (V)**	**FF (%)**	**PCE (%)**
FOIC	1:1	/	/	2.38	0.77	51	0.94
Y6	1:1	/	/	7.44	0.69	63	3.25
Y16F	1:1	/	/	3.93	0.79	47	1.46
IEICO	1:1	/	/	1.45	0.74	38	0.41
Y6	**1:1**	/	/	7.22	0.70	60	3.05
Y6	**1:1.5**	/	/	5.83	0.71	55	2.26
Y6	**1:2**	/	/	6.91	0.70	58	2.79
Y6	1:1	**1**	/	9.40	0.64	64	3.85
Y6	1:1	**3**	/	9.38	0.60	61	3.42
Y6	1:1	**5**	/	8.26	0.59	62	3.01
Y6	1:1	1	**80**	7.79	0.57	43	1.90
Y6	1:1	1	**130**	8.28	0.64	65	3.39
Y6	1:1	1	**160**	9.49	0.63	66	**3.95**

Table 4. Optimization of the photovoltaic properties for solar cells based on PDPP-3T:Y6.

Acceptor	D:A ratio (wt:wt)	CB (%)	Ann. T (°C)	J_{SC} (mA/cm^2)	V_{OC} (V)	FF (%)	PCE (%)
Y6	**1:1**	/	/	6.53	0.60	56.81	2.22
Y6	**1:1.5**	/	/	9.78	0.60	63.69	3.71
Y6	**1:2**	/	/	10.93	0.58	64.72	4.12
Y6	1:2	**1**	/	10.07	0.54	55.55	3.02
Y6	1:2	**3**	/	12.20	0.51	63.67	3.91
Y6	1:2	**5**	/	9.45	0.51	63.99	3.07
Y6	1:2	/	**80**	10.23	0.60	67.71	4.12
Y6	1:2	/	**130**	11.19	0.58	68.06	**4.45**
Y6	1:2	/	**160**	11.41	0.56	67.93	4.34

External quantum efficiencies (EQE) were also measured for the optimized solar cells based on PDPP-3T:Y6 and PDPP-3T(Cl):Y6 (**Figure 7**). For the novel PDPP-3T(Cl)-based devices the EQE is slightly lower than for the non-chlorinated PDPP-3T based solar cells. This is in good correlation with the lower J_{sc} measured for the PDPP-3T(Cl)-based cells (9.49 compared to 11.19 mA/cm^2).

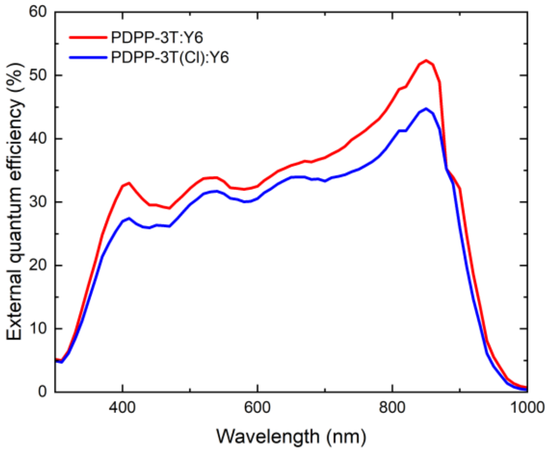

Figure 7. External quantum efficiencies of the solar cells based on the optimized blends of PDPP-3T:Y6 (red) and PDPP-3T(Cl):Y6 (blue).

3. Conclusions

Two novel NIR absorbing NFAs, DOOTIC-4F and DOTIC-4F, were successfully synthesized. By replacing the CPDT core of COTIC-4F with a stronger electron donating core (DTP(O) and DTP), the absorption of the NFA could be slightly redshifted. Unfortunately, the novel acceptors showed poor solubility in organic solvents, which led to a rough active layer, and therefore poor solar cell performances when combined with different donor polymers. To solve this, the solubility of NFAs may be improved by, for example, using extended side chains on the thiophene linkers. The novel PDPP-3T(Cl) donor polymer was also synthesized successfully with a molar mass of 26.7 kDa. Incorporating the chlorine onto the polymer backbone resulted in a lower HOMO energy level compared to PDPP-3T, while the absorption profile did not change significantly. The lower HOMO level subsequently resulted in a higher V_{OC} of 0.64 V for the PDPP-3T(Cl)-based devices, compared to 0.58 V for the PDPP- 3T-based devices. The optimized PDPP-3T(Cl):Y6 based solar cells yielded a respectable PCE of 3.95%.

4. Acknowledgements

In the first place, I would like to express my deepest appreciation to my mentor, drs Kaat Valkeneers, for providing invaluable knowledge, expertise, and guidance in this project. This dissertation would not have been possible without her feedback. I am also extremely grateful to prof. dr. Wouter Maes for giving me the opportunity to work on this project and for the help and feedback on the project and thesis. I would like to extend my sincere thanks to my copromotor, prof. dr. ir. Koen Vandewal, for his support and advice on the project. Thanks to Huguette Penxten for CV analysis, to Koen Van Vinckenroye and dr. Sander Smeets for all NMR analysis and to dr. Rachith Shanivarasanthe Nithyananda Kumar for the AFM measurements.

Thanks should also go to the members of the DSOS research team for any advice and help they have given, and for welcoming me into the group during this period. I would also like to recognize everyone who helped organize the Materiomics master, especially dr. Sarah Doumen, dr. Dorien Baeten, and prof. dr. An Hardy, for their contributions to the thesis projects as well as to the master's program.

I would also like to give a special thanks to my Materiomics classmates for their moral support and general help during this project. In particular, I thank Brent Van Ballaer, Katrien Derkoningen, and Lisa Cuypers for the fun working environment. Lastly, I have to thank my family and friends for their support and motivation during this process.

5. References

[1] IEA, World Energy Outlook 2023, Paris, **2023**.

[2] Y. Li, W. Huang, D. Zhao, L. Wang, Z. Jiao, Q. Huang, P. Wang, M. Sun, G. Yuan, *Molecules* **2022**, *27*, 1800.

[3] Y. Xie, R. Xia, T. Li, L. Ye, X. Zhan, H. L. Yip, Y. Sun, *Small Methods* **2019**, *3*, 2000136.

[4] a) P. Corti, L. Capannolo, P. Bonomo, P. De Berardinis, F. Frontini, *Energies* **2020**, *13*, 3827.
b) E. P. Thompson, E. L. Bombelli, S. Shubham, H. Watson, A. Everard, V. D'Ardes, A. Schievano, S. Bocchi, N. Zand, C. J. Howe, P. Bombelli, *Advanced Energy Materials* **2020**, *10*, 2001189.

[5] K. Lee, H.-D. Um, D. Choi, J. Park, N. Kim, H. Kim, K. Seo, *Cell Reports Physical Science* **2020**, *1*, 100143.

[6] C. J. Traverse, R. Pandey, M. C. Barr, R. R. Lunt, *Nature Energy* **2017**, *2*, 849-860.

[7] S.-Y. Chang, P. Cheng, G. Li, Y. Yang, *Joule* **2018**, *2*, 1039-1054.

[8] C. Yang, D. Liu, M. Bates, M. C. Barr, R. R. Lunt, *Joule* **2019**, *3*, 1803-1809.

[9] J. Lee, H. Cha, H. Yao, J. Hou, Y. H. Suh, S. Jeong, K. Lee, J. R. Durrant, *ACS Applied Materials & Interfaces* **2020**, *12*, 32764-32770.

[10] J. W. Yoon, H. Bae, J. Yang, J.-W. Ha, C. Lee, J. Lee, S. C. Yoon, H. Choi, S.-J. Ko, *Chemical Engineering Journal* **2023**, *452*, 139423.

[11] J. Lee, S. J. Ko, M. Seifrid, H. Lee, B. R. Luginbuhl, A. Karki, M. Ford, K. Rosenthal, K. Cho, T. Q. Nguyen, G. C. Bazan, *Advanced Energy Materials* **2018**, *8*, 1801212.

[12] Y. Chen, Y. Zheng, Y. Jiang, H. Fan, X. Zhu, *Journal of the American Chemical Society*. **2021**, *143*, 4281-4289.

[13] a) J. C. Bijleveld, A. P. Zoombelt, S. G. Mathijssen, M. M. Wienk, M. Turbiez, D. M. de Leeuw, R. A. Janssen, *Journal of the American Chemical Society* **2009**, *131*, 16616-16617;
b) J. Huang, H. Wang, K. Yan, X. Zhang, H. Chen, C. Z. Li, J. Yu, *Advanced Materials*. **2017**, *29*, 1606729.

[14] B. Tieke, A. R. Rabindranath, K. Zhang, Y. Zhu, *Beilstein Journal of Organic Chemistry*. **2010**, *6*, 830-845.

[15] K. Valkeneers, PhD thesis, University of Hasselt (Belgium), 2024.

[16] J. Lee, S.-J. Ko, H. Lee, J. Huang, Z. Zhu, M. Seifrid, J. Vollbrecht, V. V. Brus, A. Karki, H. Wang, K. Cho, T.-Q. Nguyen, G. C. Bazan, *ACS Energy Letters* **2019**, *4*, 1401-1409.

[17] a) J. Zhao, X. Xu, L. Yu, R. Li, Y. Li, Q. Peng, *ACS Applied Matererials & Interfaces* **2021**, *13*, 25214-25223;
b) X. Qin, X. Li, Q. Huang, H. Liu, D. Wu, Q. Guo, J. Lan, R. Wang, J. You, *Angewandte Chemie International Edition in English* **2015**, *54*, 7167-7170.

[18] a) S. Förtsch, P. Bäuerle, *Polymer Chemistry* **2017**, *8*, 3586-3595;
b) G. Conboy, R. G. D. Taylor, N. J. Findlay, A. L. Kanibolotsky, A. R. Inigo, S. S. Ghosh, B. Ebenhoch, L. Krishnan Jagadamma, G. K. V. V. Thalluri, M. T. Sajjad, I. D. W. Samuel, P. J. Skabara, *Journal of Materials Chemistry C* **2017**, *5*, 11927-11936.

[19] C.-W. Ge, C.-Y. Mei, J. Ling, F.-G. Zhao, H.-J. Li, L. Liang, J.-T. Wang, J.-C. Yu, W. Shao, Y.-S. Xie, W.-S. Li, *Journal of Polymer Science Part A: Polymer Chemistry* **2014**, *52*, 2356-2366.

[20] J. Qi, J. Han, X. Zhou, D. Yang, J. Zhang, W. Qiao, D. Ma, Z. Y. Wang, *Macromolecules* **2015**, *48*, 3941-3948.

Supporting Information

Materials and methods

All commercially available reagents were obtained from Abcr, Acros Organics, Alfa Aesar, Fluorochem, J&K Scientific, Sigma-Aldrich, TCI Europe, or VWR Chemicals and these were used without further purification. Solvents were acquired from Fisher Scientific, Sigma-Aldrich, or VWR Chemicals and were also used without further purification. Dry solvents were obtained from an MBraun solvent purification system (MB SPS-800) equipped with alumina columns. Nuclear magnetic resonance (NMR) spectra were obtained on a Varian or Jeol spectrometer operating at a frequency of 400 MHz for ^{1}H. Measurements were performed in deuterated chloroform ($CDCl_3$) or DMSO-d_6 and chemical shifts (δ) are given in ppm relative to $CDCl_3$ (δ = 7.26 ppm for ^{1}H NMR, δ = 77.16 ppm for ^{13}C NMR). Coupling constants are given in Hz. Matrix-assisted laser desorption/ionization - time-of-flight (MALDI–ToF) mass spectra were recorded on a Bruker Daltonics UltrafleXtreme MALDI/ToF-ToF system. 10 µL of the matrix solution (20 mg mL^{-1} *trans*-2-[3-(4-*tert*-butylphenyl)-2-methyl-2-propenylidene]malononitrile (DCTB) in chlorobenzene) was mixed with 3.5 µL analyte solution of approximately 1 mg mL^{-1} in chloroform. 1 µL of this solution was spotted onto an MTP Anchorchip 600/384 MALDI plate. Polymer molar mass distributions were estimated by size exclusion chromatography at 160 °C on an Agilent 1260 Infinity II High-Temperature GPC system using a PL-GEL 10 µm MIXED-B column with 1,2,4-trichlorobenzene as the eluent and using polystyrene internal standards. Background corrected UV-Vis-NIR absorption spectroscopy measurements were performed on a VARIAN Cary 5000 UV-Vis-NIR spectrophotometer at a scan rate of 600 nm min^{-1}. The films for the UV-Vis-NIR absorption measurements were prepared by drop-casting a solution of the respective polymer in $CHCl_3$ on a quartz substrate. Absorption coefficients were determined using the DRA 2500 internal diffuse reflectance accessory. By measuring both the transmission (T) and reflectance (R) of spincoated thin films on glass, the absorption coefficient was calculated as $\alpha = -1/d \ln (T/(100\%-R))$, hereby neglecting weak interference effects. The solid-state UV-Vis-NIR absorption spectra were used to estimate the optical gaps (from the wavelength at the intersection of the tangent line drawn at the low energy side of the absorption spectrum with the baseline: E_g (eV) = 1240/(wavelength in nm). Electrochemical measurements (cyclic voltammetry, CV) were performed with an Eco Chemie Autolab PGSTAT 30 potentiostat/galvanostat using a three-electrode microcell with a platinum working electrode, a platinum counter electrode, and a Ag/AgNO$_3$ reference electrode (silver wire dipped in a solution of 0.01 M AgNO$_3$ and 0.1 M NBu$_4$PF$_6$ in anhydrous acetonitrile). The reference electrode was calibrated against ferrocene/ferrocenium as external standard. Sample preparation was done by dip-coating the platinum working electrode in the respective polymer solutions. The CV measurements were done on the resulting films with 0.1 M NBu$_4$PF$_6$ in anhydrous acetonitrile as electrolyte solution. The experiments were carried out under a curtain of argon to prevent air from entering the system. Cyclic voltammograms were recorded at a scan rate of 100 mV s^{-1}. For the conversion of V to eV, the onset potentials of the first oxidation/reduction peaks were used and referenced to ferrocene/ferrocenium, which has an ionization potential of −4.98 eV vs. vacuum. This correction factor is based on a value of 0.31 eV for Fc/Fc$^+$ vs. SCE [1] and a value of 4.68 eV for SCE vs. vacuum [2]: $E_{\text{HOMO/LUMO}}$ (eV) = $-4.98 - E_{\text{onset ox/red Ag/AgNO3}}$ (V) + $E_{\text{onset Fc/Fc+ Ag/AgNO3}}$ (V). The accuracy of measuring redox potentials by CV is about 0.01−0.02 V. Reproducibility issues can occur due to the dependence of the potentials on concentration and temperature.

Synthesis and characterization

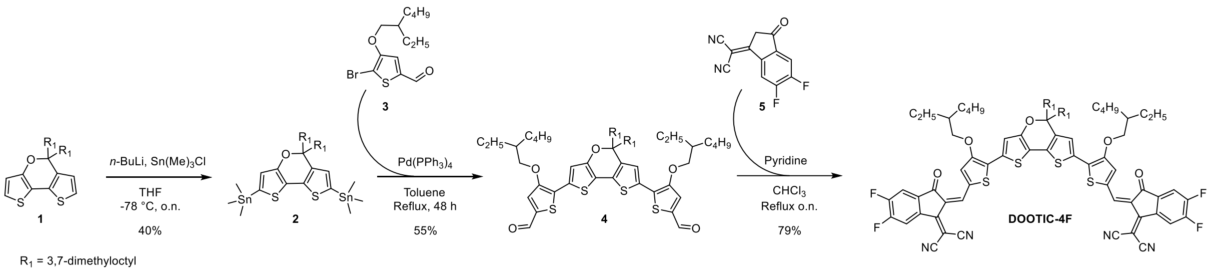

Scheme S1. Synthesis of DOOTIC-4F.

(5,5-bis(3,7-dimethyloctyl)-5*H*-dithieno[3,2-*b*:2’,3’-*d*]pyran-2,7-diyl)bis(trimethylstannane) (2)

The synthesis of (5,5-bis(3,7-dimethyloctyl)-5*H*-dithieno[3,2-b:2’,3’-*d*]pyran-2,7-diyl)bis(trimethylstannane) (**2**) was carried out following a literature procedure. [3] Yield 40%. ^{1}H-NMR (400 MHz, CDCl$_3$) δ ppm 6.72 (s, 1H), 6.69 (s, 1H), 1.91 – 1.78 (m, 4H), 1.52 – 0.99 (m, 12H), 0.85 – 0.79 (m, 18H), 0.33 (s, 18H).

5,5’-(5,5-bis(3,7-dimethyloctyl)-5*H*-dithieno[3,2-*b*:2’,3’-*d*]pyran-2,7-diyl)bis(4-((2-ethylhexyl)oxy)thiophene-2-carbaldehyde (4)

(5,5-Bis(3,7-dimethyloctyl)-5*H*-dithieno[3,2-*b*:2’,3’-*d*]pyran-2,7-diyl)bis(trimethylstannane) (**2**) (390 mg, 0.49 mmol, 1 eq), 5-bromo-4-((ethylhexyl)oxy)thiophene-2-carbaldehyde (**3**) (393 mg, 1.23 mmol, 2.5 eq), and $Pd(PPh_3)_4$ (34 mg, 0.028 mmol, 0.05 eq) were dissolved in dry toluene (9.5 mL) under Argon atmosphere and the mixture was stirred at reflux for 48 h. Water (10 mL) was added and the mixture was extracted with diethyl ether three times. The organic phases were combined, washed with water (3x), dried over $MgSO_4$, filtered and the solvent was evaporated *in vacuo.* The crude product was further purified by flash column chromatography (silica, 1:1 petroleum ether:dichloromethane to pure dichloromethane) and preparative recycling GPC (chloroform) to yield the product as a red oil (250 mg, 55%). ^{1}H-NMR (400 MHz, $CDCl_3$) δ ppm 9.74 (s, 2H), 7.45 (s+s, 2H), 7.06 (s, 1H), 6.98 (s, 1H), 4.08 (dd, *J* = 5.3, 2.3 Hz, 4H), 1.97 – 1.77 (m, 4H), 1.65 – 1.02 (m, 42H), 0.98 (t, *J* = 7.4 Hz, 6H), 0.95 – 0.90 (m, 6H), 0.84 – 0.77 (m, 18H). ^{13}C NMR (400 MHz, $CDCl_3$) δ 181.7, 181.6, 153.6, 153.1, 152.1, 136.0, 135.5, 134.3, 134.3, 134.3, 130.5, 130.2, 129.9, 126.6, 126.5, 123.4, 122.9, 115.5, 112.4, 86.9, 86.8, 74.5, 74.2, 39.8, 39.8, 39.3, 37.7, 37.6, 37.1, 36.9, 33.1, 33.0, 30.7, 30.6, 29.2, 29.2, 28.1, 24.9, 24.8, 24.1, 24.0, 23.1, 22.8, 22.7, 19.8, 14.3, 11.4, 11.3. MALDI-ToF-MS: calcd. for $C_{55}H_{82}O_5S_4$ $[M]^+$: *m/z* = 950.5, measured: *m/z* = 950.5.

2,2'-((((5,5-bis(2,7-dimethyloctyl)-5*H*-dithieno[3,2-*b*:2',3'-*d*]pyran-2,7-diyl)bis(4-((2-hexyldecyl)oxy)thiophene-5,2-diyl))bis(methylene))bis(5,6-difluoro-3-oxo-2,3-dihydro-1*H*-indene-2-yl-1-ylidene))dimalononitrile (DOOTIC-4F)

5,5’-(5,5-Bis(3,7-dimethyloctyl)-5*H*-dithieno[3,2-*b*:2’,3’-*d*]pyran-2,7-diyl)bis(4-((2-ethylhexyl)oxy)thiophene-2-carbaldehyde (**4**) (107 mg, 0.112 mmol, 1 eq), and 2-(5,6-difluoro-3-oxo-2,3-dihydro-1*H*-inden-1-ylidene)malononitrile (**5**) (103 mg, 0.448 mmol, 4 eq) were dissolved in dry chloroform (4.3 mL) under Argon atmosphere and pyridine (0,56 mL, 6.94 mmol, 62 eq) was added. The solution was refluxed overnight. Then, water was added (10 mL) and the reaction mixture was extracted with chloroform three times. The combined organic phases were washed with water three times, dried over $MgSO_4$, filtered and the solvent was removed *in vacuo*. The crude product was further purified by flash column chromatography (silica,1:1 petroleum ether:dichloromethane to pure dichloromethane) and preparative recycling GPC (chloroform) to yield the product as a blue solid (122 mg, 79%). ^{1}H-NMR (400 MHz, $CDCl_3$) δ 8.67 (s, 1H), 8.63 (s, 1H), 8.54 – 8.42 (m, 2H), 7.67 – 7.61 (m, 2H), 7.48 (s, 2H), 7.35 (s, 1H), 7.18 (s, 1H), 4.16 – 4.10 (m, 4H), 2.04 – 1.81 (m, 4H), 1.73 – 0.90 (m, 38H), 0.89 – 0.76 (m, 30H). MALDI-ToF-MS: calcd. for $C_{79}H_{86}F_4N_4O_5S_4$ $[M]^+$: *m/z* = 1374.5, measured: *m/z* = 1374.4.

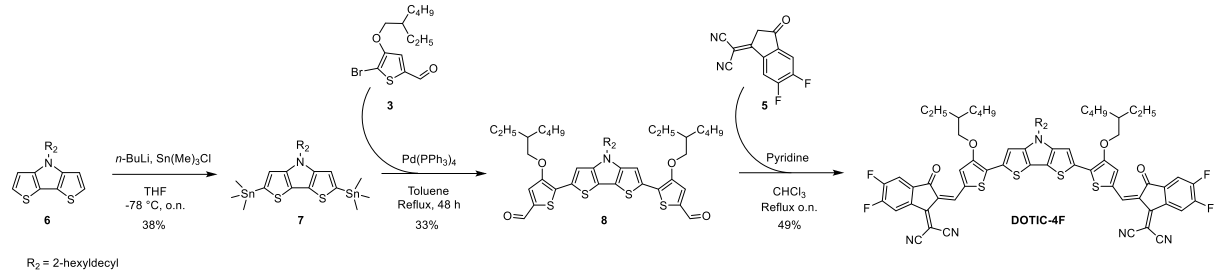

Scheme S2. Synthesis of DOTIC-4F.

4-(2-hexyldecyl)-2,6-bis(trimethylstannyl)-4*H*-dithieno[3,2-*b*:2',3'-*d*]pyrrole (7)

The synthesis of 4-(2-ethylhexyl)-2,6-bis(trimethylstannyl)-4*H*-dithieno[3,2-*b*:2',3'-*d*]pyrrole (**7**) was carried out following a literature procedure. [4] Yield 38%. ^{1}H NMR (400 MHz, $CDCl_3$) δ 6.96 (s, 2H), 4.06 – 4.01 (m, 2H), 1.99 – 1.95 (m, 1H), 1.44 – 1.22 (m, 8H), 0.95 – 0.83 (m, 6H), 0.39 (s, 18H).

5,5'-(4-(2-hexyldecyl)-4*H*-dithieno[3,2-*b*:2',3'-*d*]pyrrole-2,6-diyl)bis(4-((2-ethylhexyl)oxy)thiophene-2-carbaldehyde) (8)

4-(2-Hexyldecyl)-2,6-bis(trimethylstannyl)-4*H*-dithieno[3,2-*b*:2',3'-*d*]pyrrole (**7**) (55 mg, 75.4 µmol, 1 eq), 5-bromo-4-((ethylhexyl)oxy)thiophene-2-carbaldehyde (**3**) (60.2 mg, 0.189 mmol, 2.5 eq), and $Pd(PPh_3)_4$ (4.36 mg, 3.77 µmol, 0.05 eq) were dissolved in dry toluene (2.5 mL) under Argon atmosphere and the mixture was stirred at reflux for 48 h. Water (2.5 mL) was added and the mixture was extracted with diethyl ether three times. The organic phases were combined, washed with water (3x), dried over $MgSO_4$, filtered and the solvent was evaporated *in vacuo.* The crude product was further purified by flash column chromatography (silica, 1:1 petroleum ether:dichloromethane to pure dichloromethane) and preparative recycling GPC (chloroform) to yield the product as a red oil (22 mg, 33%) ^{1}H NMR (400 MHz, $CDCl_3$) δ 9.73 (s, 2H), 7.46 (s, 2H), 7.32 (s, 2H), 4.10 (d, *J* = 5.3 Hz, 4H), 4.01 (d, *J* = 7.5 Hz, 2H), 2.04 – 1.95 (m, 1H), 1.90 – 1.78 (m, 2H), 1.71 – 1.13 (m, 40H) 1.03 – 0.78 (m, 18H).

2,2'-((2*Z*,2'*Z*)-(((4-(2-hexyldecyl)-4*H*-dithieno[3,2-*b*:2',3'-*d*]pyrrole-2,6-diyl)bis(4-((2-ethylhexyl)oxy)thiophene-5,2-diyl))bis(methaneylylidene))bis(5,6-difluoro-3-oxo-2,3-dihydro-1*H*-indene-2,1-diylidene))dimalononitrile (DOTIC-4F)

5,5'-(4-(2-Hexyldecyl)-4*H*-dithieno[3,2-*b*:2',3'-*d*]pyrrole-2,6-diyl)bis(4-((2-ethylhexyl)oxy)-thiophene-2-carbaldehyde) (**8**) (22 mg, 25 µmol, 1 eq) and 2-(5,6-difluoro-3-oxo-2,3-dihydro-1*H*-inden-1-ylidene)malononitrile (**5**) (23 mg, 0.10 mmol, 4 eq) were dissolved in dry chloroform (0.9 mL) under Argon atmosphere and pyridine (0.13 mL, 1.5 mmol, 62 eq) was added. The solution was refluxed overnight. Then, water was added (2.5 mL) and the reaction mixture was extracted with chloroform three times. The combined organic phases were washed with water three times, dried over $MgSO_4$, filtered and the solvent was removed *in vacuo*. The crude product was further purified by flash column chromatography (silica, 1:1 petroleum ether:dichloromethane to pure dichloromethane) and preparative recycling GPC (chloroform) to yield the product as a blue solid (16 mg, 49%). ^{1}H-NMR (400 MHz, $CDCl_3$) δ 8.61 (s, 2H), 8.48 – 8.40 (m, 2H), 7.65 – 7.55 (m, 2H), 7.47 (s, 2H), 7.35 (s, 1H), 4.23 – 4.11 (m, 4H), 4.08 – 3.98 (m, 2H), 1.78 – 1.52 (m, 5H), 1.50 – 1.12 (m, 40H), 1.10 – 0.76 (m, 18H). MALDI-ToF-MS: calcd. for $C_{74}H_{77}F_4N_5O_4S_4$ $[M]^+$: *m/z* = 1303.5, measured: *m/z* = 1304.6.

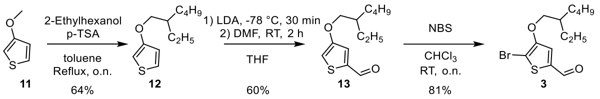

Scheme S3. Synthesis of 5-bromo-4-((2-ethylhexyl)oxy)thiophene-2-carbaldehyde (**3**).

3-((2-ethylhexyl)oxy)thiophene (12)

The synthesis of 4-((2-ethylhexyl)oxy)thiophene-2-carbaldehyde (**12**) was carried out following a literature procedure. [5] Yield: 64%. ^{1}H NMR (400 MHz, $CDCl_3$) δ 7.15 (dd, *J* = 5.2, 3.1 Hz, 1H), 6.74 (dd, *J* = 5.2, 1.5 Hz, 1H), 6.21 (dd, *J* = 3.1, 1.5 Hz, 1H), 3.85 – 3.78 (m, 2H), 1.74 – 1.63 (m, 1H), 1.52 – 1.23 (m, 8H), 0.95 – 0.82 (m, 6H).

4-((2-ethylhexyl)oxy)thiophene-2-carbaldehyde (13)

The synthesis of 4-((2-ethylhexyl)oxy)thiophene-2-carbaldehyde (**13**) was carried out following a literature procedure. [6] Yield: 60%. ^{1}H NMR (400 MHz, $CDCl_3$) δ 9.80 (d, *J* = 1.2 Hz, 1H), 7.40 (d, *J* = 1.7 Hz, 1H), 6.71 (dd, *J* = 1.7, 1.2 Hz, 1H), 3.88 – 3.81 (m, 2H), 1.75 – 1.64 (m, 1H), 1.52 – 1.22 (m, 8H), 0.95 – 0.85 (m, 6H).

5-bromo-4-((2-ethylhexyl)oxy)thiophene-2-carbaldehyde (3)

The synthesis of 5-bromo-4-((2-ethylhexyl)oxy)thiophene-2-carbaldehyde **(3)** was carried out following a literature procedure. [6] Yield: 81%. ^{1}H NMR (400 MHz, CDCl$_3$) δ 9.69 (s, 1H), 7.36 (s, 1H), 3.95 (d, *J* = 5.8 Hz, 2H), 1.77 – 1.66 (m, 1H), 1.54 – 1.25 (m, 8H), 0.85 – 0.97 (m, 6H).

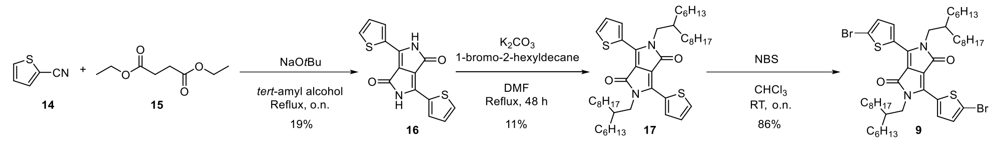

Scheme S4. Synthesis of diketopyrrolopyrrole **9**. [7]

3,6-di(thiophen-2-yl)-2,5-dihydropyrrolopyrrolo[3,4-*c*]pyrrole-1,4-dione (16)

The synthesis of 3,6-di(thiophen-2-yl)-2,5-dihydropyrrolopyrrolo[3,4-*c*]pyrrole-1,4-dione (**16**) was carried out following a literature procedure. [7] Yield 19%. ^{1}H NMR (400 MHz, DMSO-*d*$_6$) δ 11.25 (s, 2H), 8.21 (dd, *J* = 3.8, 1.2 Hz, 2H), 7.96 (dd, *J* = 5.0, 1.1 Hz, 2H), 7.30 (dd, *J* = 5.0, 3.8 Hz, 2H).

2,5-bis(2-hexyldecyl)-3,6-di(thiophen-2-yl)-2,5-dihydropyrrolo[3,4-*c*]pyrrole-1,4-dione (17)

The synthesis of 2,5-bis(2-hexyldecyl)-3,6-di(thiophen-2-yl)-2,5-dihydropyrrolo[3,4-*c*]-pyrrole-1,4-dione (**17**) was carried out following a literature procedure. [7] Yield 11%. ^{1}H NMR (400 MHz, CDCl$_3$) δ 8.85 (dd, *J* = 3.9, 1.2 Hz, 2H), 7.61 (dd, *J* = 5.0, 1.2 Hz, 2H), 7.25 (dd, *J* = 5.0, 3.9 Hz, 2H), 4.00 (d, *J* = 7.7 Hz, 4H), 1.94 – 1.83 (m, 2H), 1.36 – 1.09 (m, 48H), 0.91 – 0.76 (m, 12H).

3,6-bis(5-bromothiophen-2-yl)-2,5-bis(2-hexyldecyl)-2,5-dihydropyrrolo[3,4-*c*]pyrrole-1,4-dione (9)

The synthesis of 3,6-bis(5-bromothiophen-2-yl)-2,5-bis(2-hexyldecyl)-2,5-dihydropyrrolo[3,4-*c*]pyrrole-1,4-dione (**9**) was carried out following a literature procedure. [7-8] Yield 86%. ^{1}H NMR (400 MHz, CDCl$_3$) δ 8.61 (d, *J* = 4.2 Hz, 2H), 7.21 (d, *J* = 4.2 Hz, 2H), 3.91 (d, *J* = 7.8 Hz, 4H), 1.87 (s, 2H), 1.37 – 1.11 (m, 48H), 0.93 – 0.74 (m, 12H).

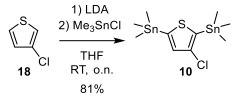

Scheme S5. Synthesis of (3-chlorothiophene-2,5-diyl)bis(trimethylstannane) (**10**).

(3-chlorothiophene-2,5-diyl)bis(trimethylstannane) (10)

3-Chlorothiophene (**18**) (110 mg, 0.91 mmol, 1 eq) was dissolved in 6 mL of dry degassed THF under Argon atmosphere. The solution was cooled to -78 °C and lithium diisopropylamide (2 M in THF, 1.6 mL, 3.2 mmol, 3.5 eq) was added dropwise. The solution was stirred for 1 h at -78 °C and thereafter stirred for 2 h while the temperature rose to -20 °C. The solution was subsequently cooled again to -78 °C, Me_3SnCl (1 M in THF, 3.6 mL, 3.6 mmol, 4 eq) was added dropwise and the solution was stirred overnight at room temperature. Afterwards, water was added and the mixture was washed with water (3x). The organic layer was dried over $MgSO_4$, filtered and the solvent was removed *in vacuo*. The crude product was purified by preparative recycling GPC, after which the pure product was obtained as a pink oil (328 mg, 81%). ^1H NMR (400 MHz, $CDCl_3$) δ 7.11 (s, 1H), 0.41 (s, 9H), 0.35 (s, 9H).

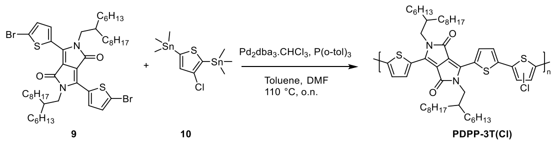

Scheme S6. Polymerization strategy for PDPP-3T(Cl).

PDPP-3T(Cl)

3,6-Bis(5-bromothiophen-2-yl)-2,5-bis(2-hexyldecyl)-2,5-dihydropyrrolo[3,4-*c*]pyrrole-1,4-dione (**9**) (0.130 g, 0.14 mmol, 1 eq), (3-chlorothiophene-2,5-diyl)bis(trimethylstannane) (**10**) (62 mg, 0.14 mmol, 1 eq), Pd_2dba_3 (4.3 mg, 4.2 µmol, 0.03 eq), and P(*o*-tol)$_3$ (5.5 mg, 18 µmol, 0.13 eq) were dissolved in a, degassed mixture of dry toluene and dry DMF under Argon atmosphere. The mixture was stirred for 64 h at 110 °C. Afterwards, the reaction mixture was cooled down to 90 °C, a spatula point of diethylammonium diethyldithiocarbamate was added, and the mixture was stirred for 1 h at 90 °C. The reaction mixture was subsequently cooled to room temperature, poured out in methanol and filtered in a thimble. The product was purified by repetitive Soxhlet extractions using methanol, acetone, *n*-hexanes, DCM, and chloroform. The chloroform fraction was concentrated, precipitated in methanol, filtered and dried, to afford a dark green-blue solid (M_n = 26.7 kDa, $Đ$ = 1.9).

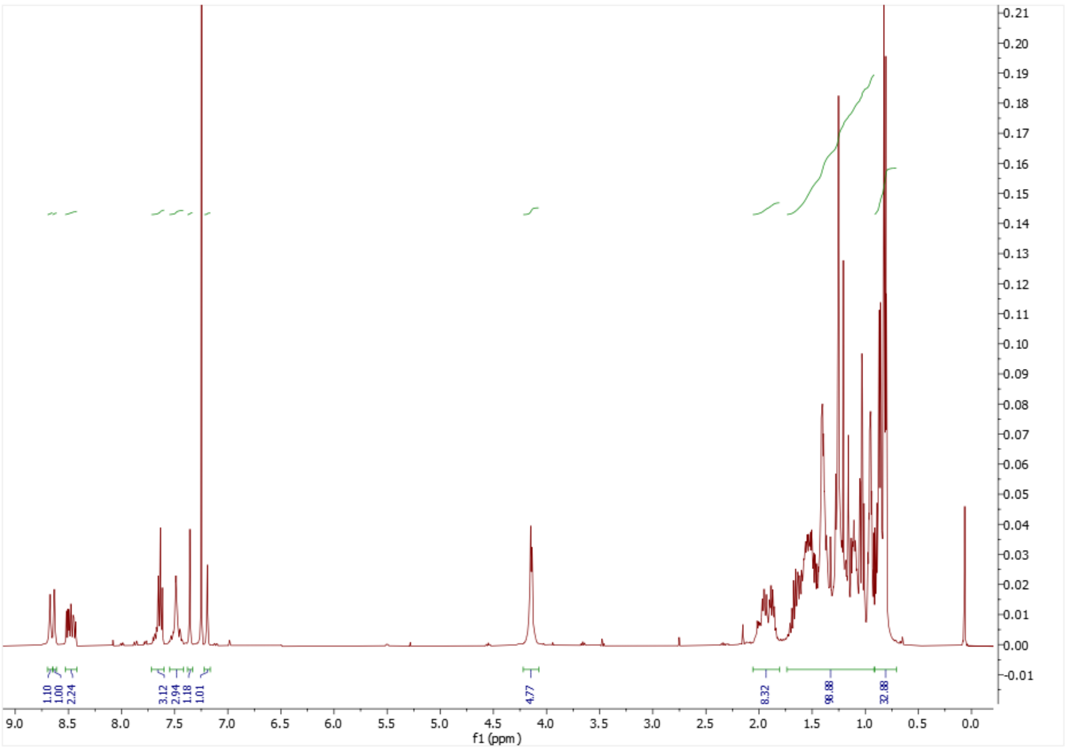

Figure S1. ^{1}H-NMR spectrum of DOOTIC-4F in $CDCl_3$.

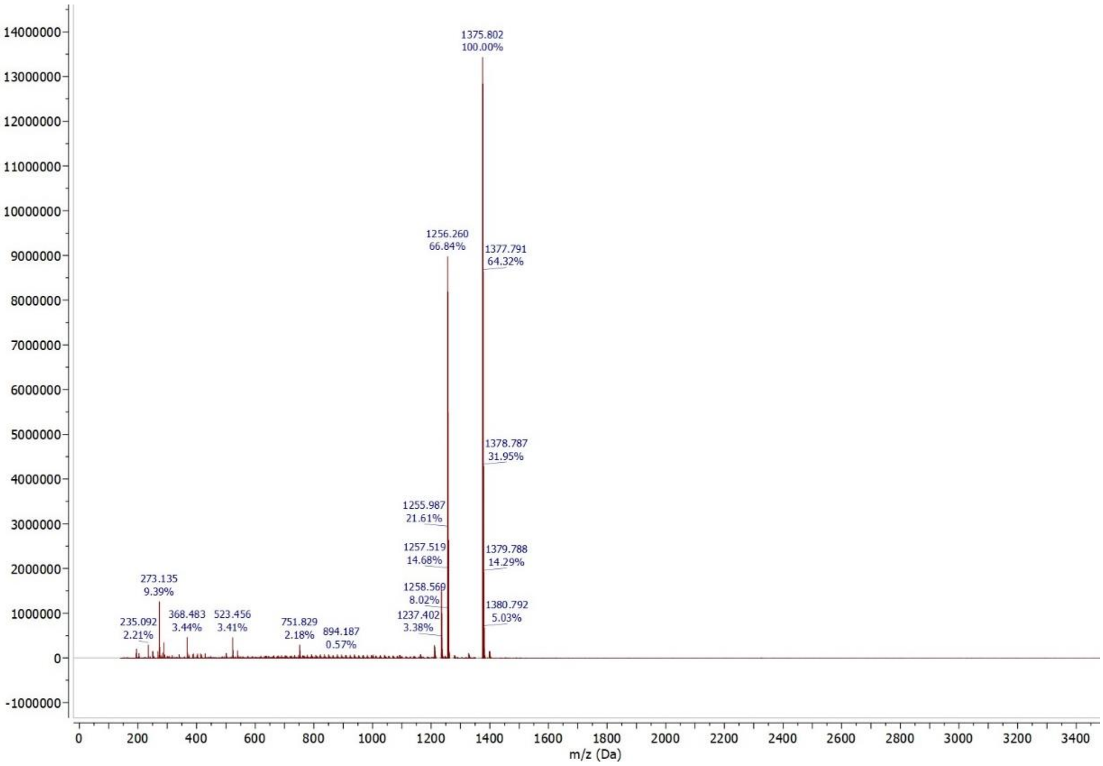

Figure S2. MALDI-ToF mass spectrum of DOOTIC-4F.

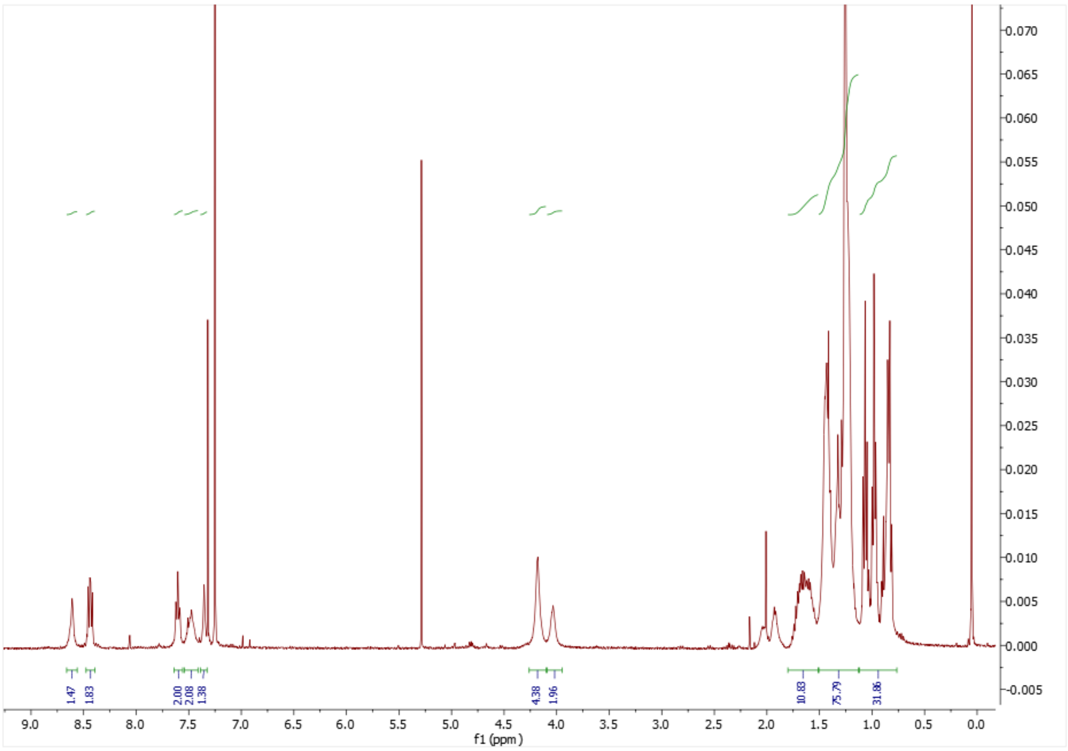

Figure S3. ^{1}H-NMR spectrum of DOTIC-4F in $CDCl_3$.

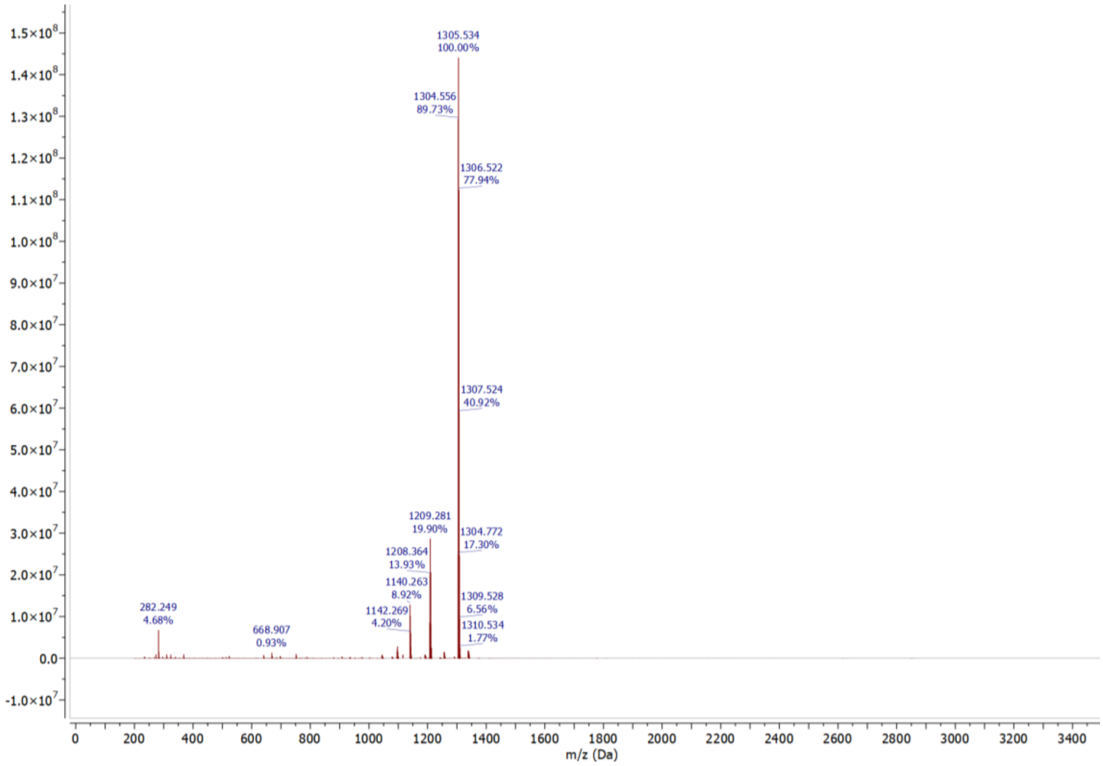

Figure S4. MALDI-ToF mass spectrum of DOTIC-4F.

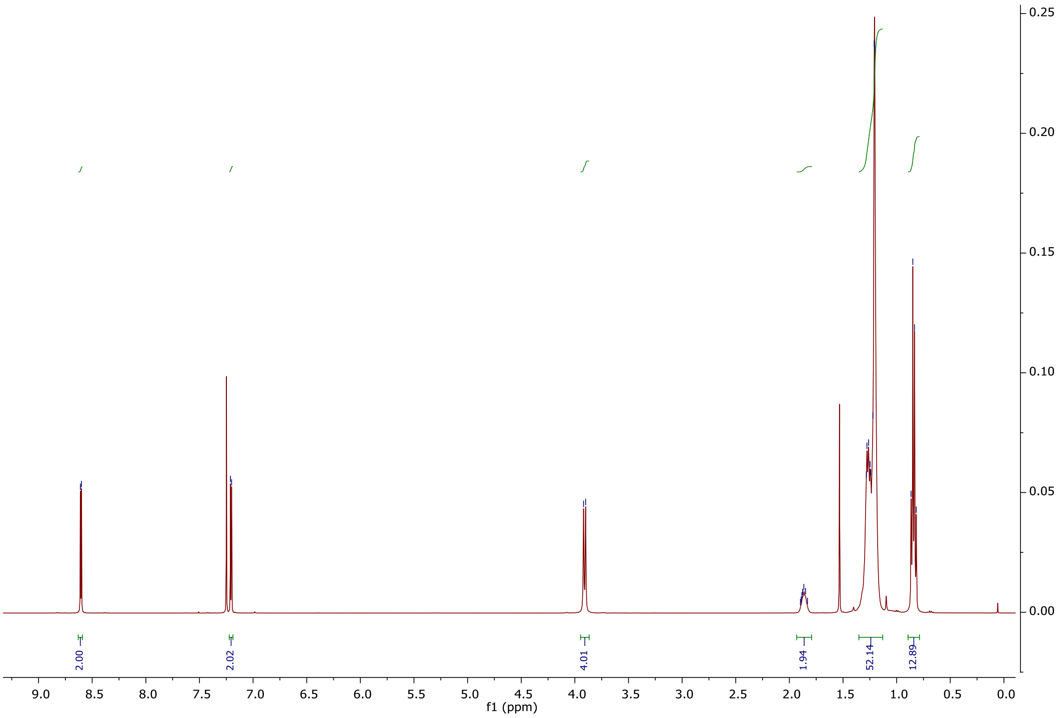

Figure S5. ^{1}H-NMR spectrum of 3,6-bis(5-bromothiophen-2-yl)-2,5-bis(2-hexyldecyl)-2,5-dihydropyrrolo[3,4-*c*]pyrrole-1,4-dione (**9**) in $CDCl_3$.

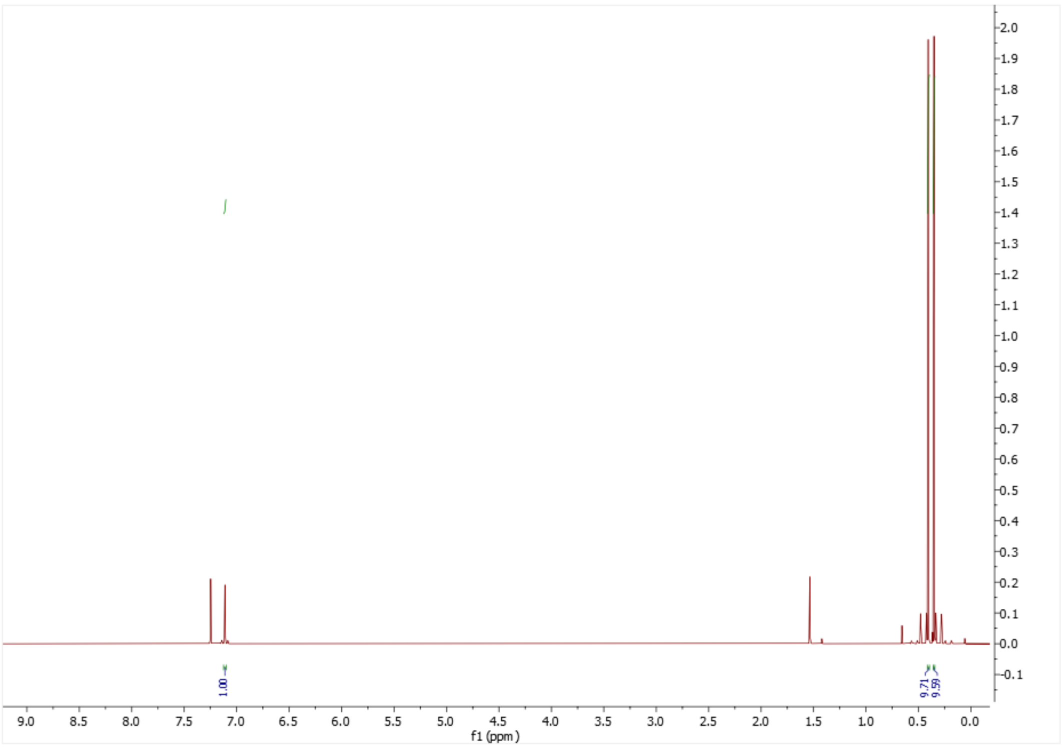

Figure S6. ^{1}H-NMR spectrum of (3-chlorothiophene-2,5-diyl)bis(trimethylstannane) (**10**) in $CDCl_3$.

Table S1. Reaction conditions and resulting molar masses for the polymerization of PDPP-3T(Cl).

Sample	Reaction time (h)	Concentration* (M)	M_n (kDa)	Đ	Collected Soxhlet fraction
PDPP-3T(Cl) 1	64	0.52	18.6	1.9	CH_2Cl_2
PDPP-3T(Cl) 2	18	0.26	18.4	1.9	CH_2Cl_2
PDPP-3T(Cl) 3	64	0.26	26.7	1.9	$CHCl_3$

*Concentration is calculated as the sum of the molarities of both monomers to the volume of solvent.

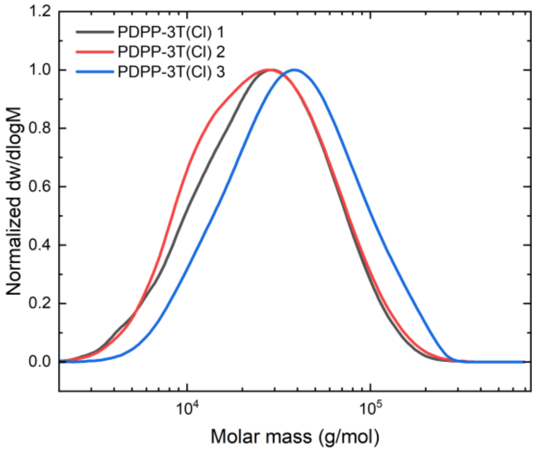

Figure S7. Molar mass distributions of the three PDPP-3T(Cl) samples measured *via* high-temperature gel permeation chromatography.

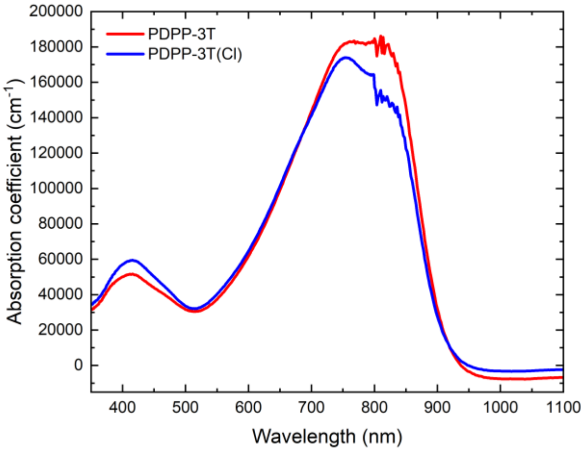

Figure S8. Absorption coefficients for PDPP-3T (red) and PDPP-3T(Cl) (blue).

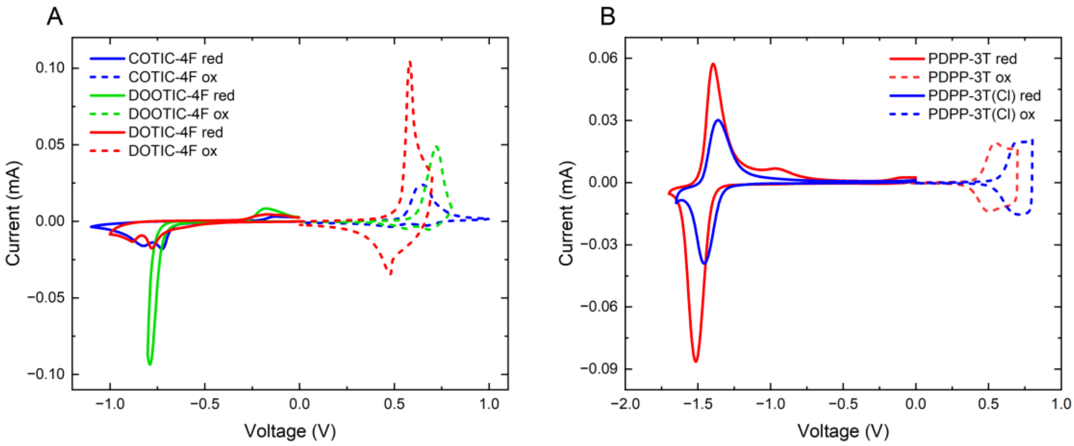

Figure S9. Reduction (solid lines) and oxidation curves (dashed lines) (A) for COTIC-4F (blue), DOOTIC-4F (green) and DOTIC-4F (red) and (B) for PDPP-3T (red) and PDPP-3T(Cl) (blue).

Device manufacturing and characterization

Bulk heterojunction organic solar cell devices were prepared using the inverted architecture glass/ITO/ZnO/active layer/MoO_3/Ag. The ITO (indium-tin-oxide) coated substrates (100 nm, Kintec, sheet resistivity 20 Ω sq^{-1}) were thoroughly cleaned *via* sonication in acetone, followed by a UV/O_3 treatment for 30 min. ZnO was deposited by spin-coating with a layer thickness of ~20 nm. The ZnO layer was annealed at 200 °C for 20 min. Further processing was performed under nitrogen atmosphere in a glove box (< 1 ppm O_2 and H_2O). The different active layers were deposited from solution as mentioned below. Finally, the MoO_3 (10 nm) hole transporting layer and Ag (100 nm) top electrode were sequentially deposited on top of the active layer through a shadow mask by thermal evaporation ($< 5 \times 10^{-6}$ mbar) to afford photovoltaic devices with an active area of 0.8 mm^2.

For COTIC-4F and DOOTIC-4F: The photoactive layer solution, consisting of the donor polymer (PTB7-Th, PDPP-3T, or PDPP-3T(Cl)) and acceptor, was spincoated from chlorobenzene. The best performing devices were obtained with a blend solution of 1:1.5 (wt/wt) donor:NFA, with a total concentration of 20 mg mL^{-1} in chlorobenzene and using 2 wt% chloronaphthalene as an additive. The solution was stirred overnight at 80 °C to ensure complete dissolution.

For PDPP-3T and PDPP-3T(Cl): The photoactive layer solution, consisting of the donor polymer (PDPP-3T or PDPP-3T(Cl)) and acceptor (FOIC, Y6, Y16F, or IEICO), was spincoated from chloroform. The best performing devices using PDPP-3T were obtained with a blend solution of 1:2 (wt/wt) donor:Y6, with a total concentration of 10 mg mL^{-1} in chloroform. After spincoating, the active layer was annealed at 130 °C for 7 minutes. The best performing devices using PDPP-3T(Cl) were obtained with a blend solution of 1:1 (wt/wt) donor:Y6, with a total concentration of 10 mg mL^{-1} in chloroform and using 1 wt% chlorobenzene as an additive. After spincoating, the active layer was annealed at 130 °C for 7 minutes. All solutions were stirred overnight at 40 °C to ensure complete dissolution.

The freshly fabricated devices were measured in an inert atmosphere and *J-V* curves (forward scan with a step of 40 mV) were recorded using a Keithley 2400 Source Meter under AM1.5 1-sun illumination, provided by a solar simulator (Newport 91195A) with a silicon calibrated intensity equivalent to 100 mW/cm^2. The EQE$_{PV}$ spectrum for the best performing cells was measured under chopped (123 Hz) monochromatic illumination from a Xe lamp (100 W, Newport) modulated by a Newport Cornerstone™ 130° Monochromator and an optical wheel chopper. The generated photocurrent from the solar cells was amplified with a Stanford Research System Model SR830 lock-in amplifier, and a calibrated silicon FDS100-CAL photodiode was employed as a reference cell. Atomic force microscopy (AFM) experiments were performed (on the devices used for the *J-V* measurements) with a JPK NanoWizard 3 AFM (JPK Instruments AG, Berlin, Germany) using AC mode in air. Silicon ACTA-50 tips from AppNano with cantilever length of ~125 mm, spring constant of ~40 N m^{-1} and resonance frequency of ~300 kHz were used. The scan angle, set point height, gain values, and scan rate were adjusted according to the calibration of the AFM tip.

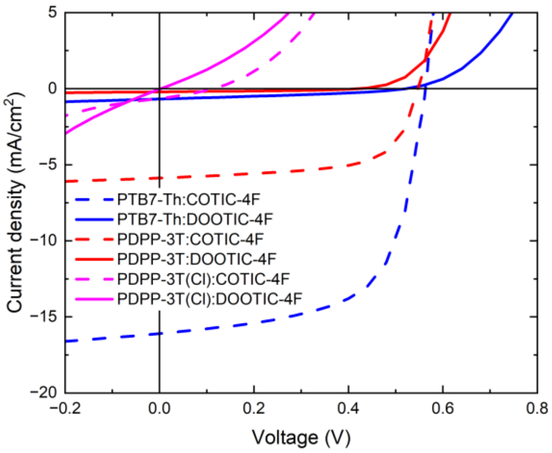

Figure S10. Current density-voltage curves for the OSCs based on COTIC-4F (dashed lines) and DOOTIC-4F (solid lines) with donor polymers PTB7-Th (blue), PDPP-3T (red), and PDPP-3T(Cl) (pink).

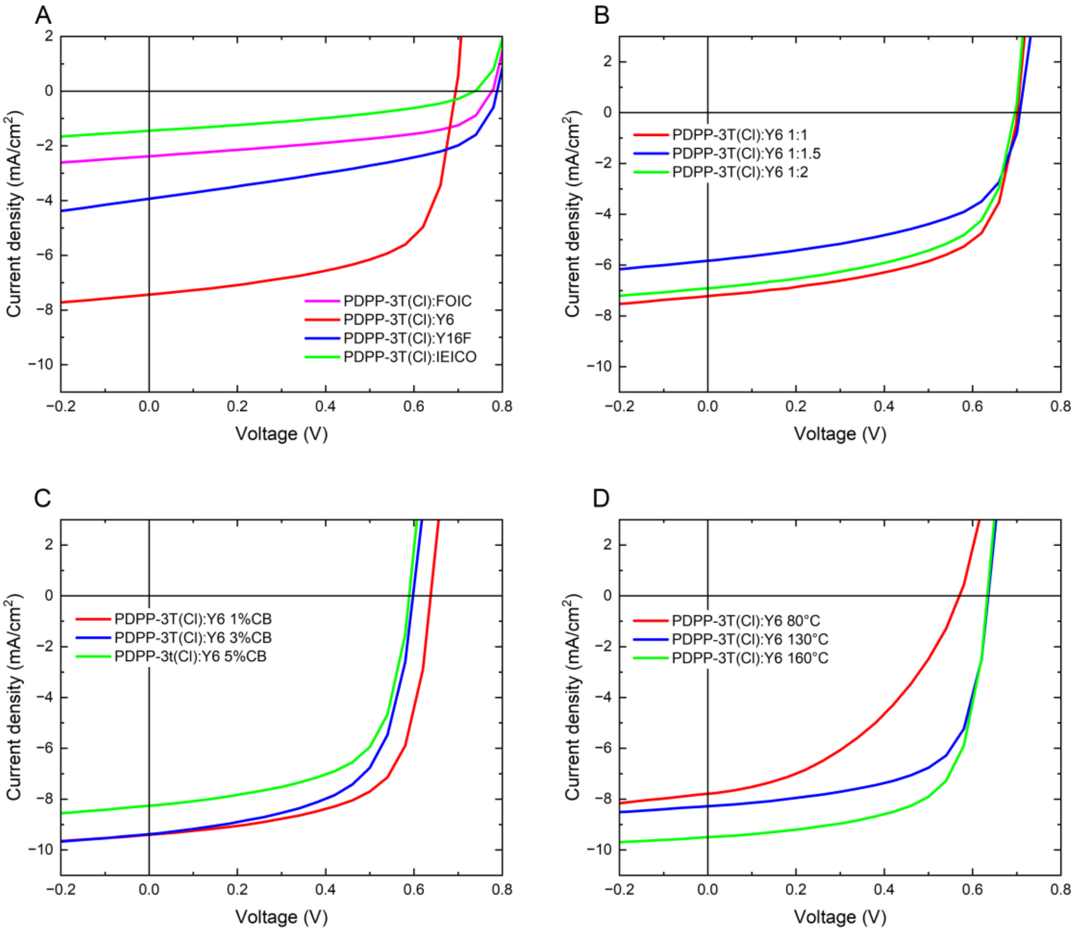

Figure S11. Current density-voltage curves for the PDPP-3T(Cl) solar cell optimization, with varying (A) acceptor material, (B) D:A ratio, (C) weight percentage chlorobenzene, and (D) annealing temperature.

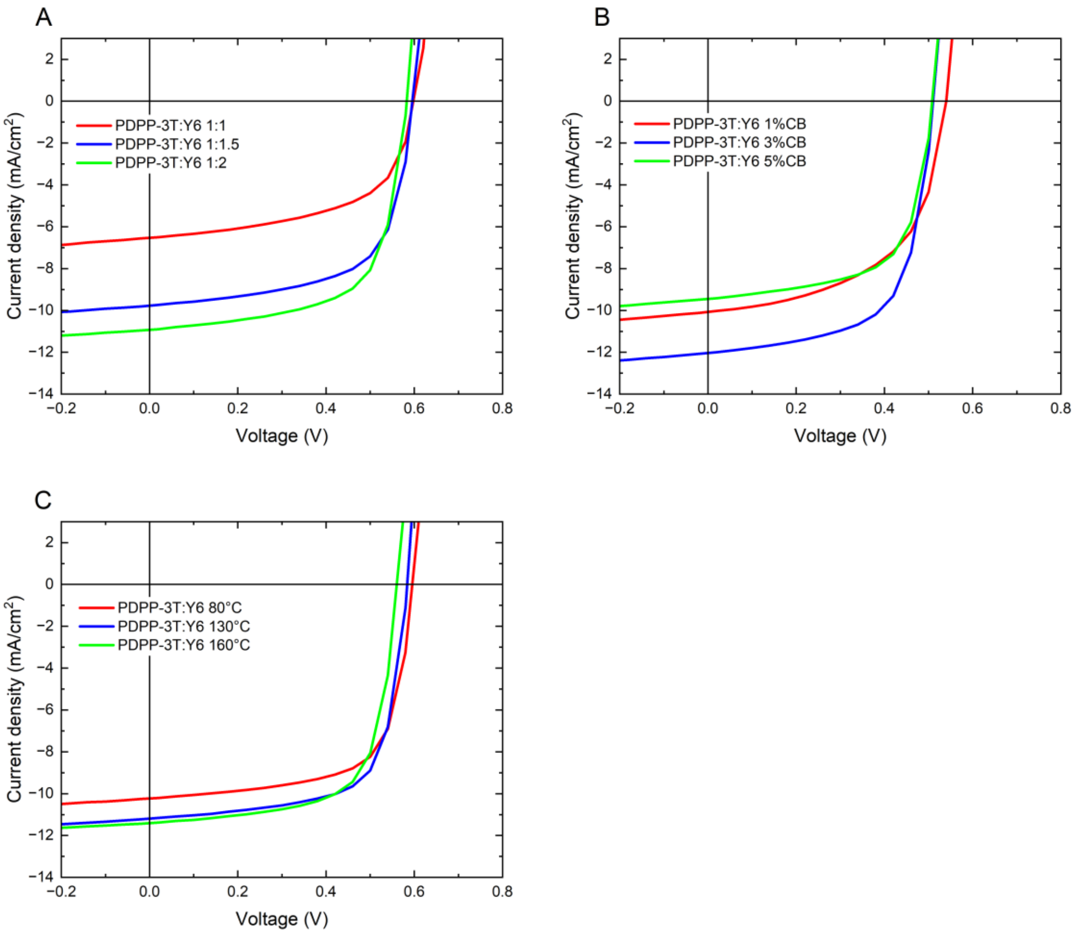

Figure S12. Current density-voltage curves for the PDPP-3T solar cell optimization, with varying (A) D:A ratio, (B) weight percentage chlorobenzene, and (C) annealing temperature.

References

[1] S. Trasatti, *Pure and Applied Chemistry* **1986**, *58*, 955-966.

[2] A. J. Bard, L. R. Faulkner, *Electrochemical methods* **2001**, *2*, 580-632.

[3] L. Dou, C.-C. Chen, K. Yoshimura, K. Ohya, W.-H. Chang, J. Gao, Y. Liu, E. Richard, Y. Yang, *Macromolecules* **2013**, *46*, 3384-3390.

[4] M. M. Shi, D. Deng, L. Chen, J. Ling, L. Fu, X. L. Hu, H. Z. Chen, *Journal of Polymer Science Part A: Polymer Chemistry* **2011**, *49*, 1453-1461.

[5] J. Vanderspikken, Q. Liu, Z. Liu, T. Vandermeeren, T. Cardeynaels, S. Gielen, B. Van Mele, N. Van den Brande, B. Champagne, K. Vandewal, W. Maes, *Advanced Functional Materials* **2021**, *32*, 2108146.

[6] X. Ji, T. Zhou, X. Ke, W. Wang, S. Wu, M. Zhang, D. Lu, X. Zhang, Y. Liu, *Journal of Materials Chemistry A* **2020**, *8*, 5163-5170.

[7] J. Qi, J. Han, X. Zhou, D. Yang, J. Zhang, W. Qiao, D. Ma, Z. Y. Wang, *Macromolecules* **2015**, *48*, 3941-3948.

[8] H. Zhu, W. Huang, Y. Huang, J. Yang, W. Wang, *Dyes and Pigments* **2016**, *127*, 37-44.